Progress toward optimal quantum tomography with unbalanced homodyning

Y. S. Teo,[1] H. Jeong,[2] and L. L. Sánchez-Soto[3,4,*]

[1]*BK21 Frontier Physics Research Division, Seoul National University, 08826 Seoul, South Korea*

[2]*Center for Macroscopic Quantum Control, Seoul National University, 08826 Seoul, South Korea*

[3]*Departamento de Óptica, Facultad de Física, Universidad Complutense, 28040 Madrid, Spain*

[4]*Max-Planck-Institut für die Physik des Lichts, Staudtstraße 2, 91058 Erlangen, Germany*

(Received 1 June 2017; published 25 October 2017)

Balanced homodyning, heterodyning, and unbalanced homodyning are three well-known sampling techniques used in quantum optics to characterize photonic sources in the continuous-variable regime. We show that for all quantum states and all observable-parameter tomography schemes, which includes reconstructions of arbitrary operator moments and phase-space quasidistributions, localized sampling with unbalanced homodyning is always tomographically more powerful (gives more accurate estimators) than delocalized sampling with heterodyning. The latter is recently known to often give more accurate parameter reconstructions than conventional marginalized sampling with balanced homodyning. This result also holds for realistic photodetectors with subunit efficiency. With examples from first- through fourth-moment tomography, we demonstrate that unbalanced homodyning can outperform balanced homodyning when heterodyning fails to do so. This new benchmark takes us one step towards optimal continuous-variable tomography with conventional photodetectors and minimal experimental components.

DOI: 10.1103/PhysRevA.96.042333

I. INTRODUCTION

In pursuing a secure information age, successful implementations of state-of-the-art continuous-variable (CV) quantum information and communication protocols [1–7] require precise reconstructions and calibrations of important properties of photonic sources. In the language of phase space quasidistributions that completely characterize such sources, these properties—generally the expectation values of quantum observables—can be reconstructed with either the physical probabilities of a positive distribution or those derived from some aspects of a (nonsingular) quasidistribution.

There are three sampling methods that identify these two main scenarios. The first, and arguably the most popular, method is *marginalized phase-space sampling* by balanced homodyne detection (BHOM) [8–12], which samples the marginal distributions of the Wigner function defined by quadrature directions. This requires a balanced (1:1) beam splitter (BS), a local oscillator (LO), and two photodetectors to measure photocurrent differences at the output. The second method is *delocalized phase-space sampling* executed with heterodyne detection (HET), which jointly measures complementary quadrature operators [13–21]. This technique randomly samples the whole phase space according to the Husimi function and usually involves a more sophisticated setup of three balanced BSs, an LO, and four photodetectors to realize such a double-BHOM scheme. The third sampling method of focus here is *localized phase-space sampling* with unbalanced homodyne detection (UHOM) [22–28], which measures displaced Fock states using a highly transmissive BS, an LO, and two photodetectors such that the Wigner function can be directly reconstructed through the parity-operator measurement. With common photodetectors that have no photon-number resolution capabilities, this method samples the Husimi function by counting "no-click" events at the transmission arm of the signal. The displacement operation by the unbalanced BS then guarantees coherent-state measurements of specified amplitudes, which data follow a binomial distribution characterized by the Husimi function at each amplitude.

The understanding of the reconstruction accuracies for all sampling methods holds a fundamental link to the tomographic power of quantum measurement schemes. There exists a plethora of articles [14,20,21,29] investigating variances and measurement uncertainties, which supply information about important statistical behaviors of parameter estimators. For the purpose of analyzing tomographic power, optimality analysis for true-parameter reconstructions is in order. Recently, the relationship between the Haar-averaged Cramér-Rao bound and the permutation group was studied in [30] and [31]. In [32–34], we systematically analyzed the tomographic power of both BHOM and HET and found that the latter gives higher reconstruction accuracies for typically interesting states, with Gaussian states being one important class in CV quantum information processing [2,35–39]. This provided irrefutable evidence of tomographic differences in parameter reconstruction for the Wigner and Husimi representations, despite their equivalence in state representation.

It is shown here that for every used reconstruction datum, localized sampling with UHOM is always tomographically more powerful than delocalized sampling with HET for *any* type of observable-parameter tomography. This benefit originates from the statistical nature of the UHOM data collected at each phase-space value. We demonstrate that this effect can even result in a superior tomographic power over BHOM in some cases where HET is inferior. These two main results are analyzed for first- through fourth-order moment tomography with Gaussian and Fock states.

II. PARAMETERS AND TOMOGRAPHIC POWER

For a more concrete concept of comparing different measurement schemes, we consider the statistical mean squared

*lsanchez@fis.ucm.es

error (MSE) $\mathbb{E}[(\widehat{\boldsymbol{q}}-\boldsymbol{q})^2]$ for any column $\boldsymbol{q}$ of parameters and its estimator $\widehat{\boldsymbol{q}}$. This accuracy measure is a function of both the measurement and the data for $\widehat{\boldsymbol{q}}$. We consider *observable parameters* of the kind $\boldsymbol{q}=\langle \boldsymbol{V}\rangle$ for an arbitrary column $\boldsymbol{V}$ of observables describing some list of quantum properties (which is a function of the position X and momentum P operators [40]) where, equivalently [41],

$$\boldsymbol{q}=\int \frac{(d\alpha')}{\pi} W(\alpha')\boldsymbol{v}_{\rm W}(\alpha') = \int \frac{(d\alpha')}{\pi} Q(\alpha')\boldsymbol{v}_{\rm P}(\alpha') \quad (1)$$

is the phase-space average of either the Glauber-Sudarshan function $\boldsymbol{v}_{\rm P}(\alpha)$ or the Wigner function $\boldsymbol{v}_{\rm W}(\alpha)=2\int(d\alpha')\,e^{-2|\alpha-\alpha'|^2}\boldsymbol{v}_{\rm P}(\alpha')/\pi$ for $\boldsymbol{V}$, respectively, with the Husimi and Wigner functions for state ρ [$0\leqslant Q(\alpha)\leqslant 1$, $-2\leqslant W(\alpha)\leqslant 2$ according to the definitions in Eq. (1)]. Each point (x,p) in phase space is expressed as $\alpha=(x+ip)/2$, and $(d\alpha)=dx\,dp/2$. Equation (1) covers all the interesting tomography problems. For instance, in second-moment tomography where $\boldsymbol{V}$ consists of symmetrically ordered products of X and P, then $\boldsymbol{v}_{\rm W}(\alpha')=(x'^2,x'p',p'^2)^{\rm T}$ and $\boldsymbol{v}_{\rm P}(\alpha')=(x'^2-1/2,x'p',p'^2-1/2)^{\rm T}$. As another example, if one is interested in Wigner function reconstruction, then $\boldsymbol{v}_{\rm W}(\alpha')=\delta(\boldsymbol{\alpha}-\alpha')$ and $\boldsymbol{v}_{\rm P}(\alpha')$ is the kernel for the Gaussian deconvolution. For an s-ordered quasidistribution, $\boldsymbol{v}_{\rm W}(\alpha')$ and $\boldsymbol{v}_{\rm P}(\alpha')$ are the relevant s-ordered kernels [42].

The detection schemes for all three sampling methods have very different kinds of data. The data sample size N for BHOM is the total number of marginalized Wigner data points defined by the sampled LO phases and real voltages. For HET and UHOM, N is the total number of randomly sampled phase-space values. In particular, we note that the relevant data for UHOM in the absence of photon counting are the "no-click" data for the D1 photodetector. For each α, these data are collected in the limit of a large fixed total number N_0 of sampling events at the transmitted arm for the signal (see Fig. 1). In this limit, the no-click data encode information about the Husimi function $Q(\alpha)$ of ρ and may be used for its reconstruction. The total number of used data copies N therefore becomes a sum of binomial random integers for every α and is itself random.

To make a fair comparison of the three schemes, the well-known (scaled) Cramér-Rao bound

$$\mathrm{sCRB}=\inf_{\widehat{\boldsymbol{q}}}\{\mathbb{E}[N(\widehat{\boldsymbol{q}}-\boldsymbol{q})^2]\} \quad (2)$$

is a good measure for the tomographic power of the measurement, which indicates the difficulty for the MSE to approach 0. This scaled measure consistently weights each experiment with its total sample size to average away the data aspect and is minimized over all conceivable reconstruction strategies for $\widehat{\boldsymbol{q}}$ of some given data type. A smaller sCRB implies a greater tomographic power.

For BHOM and HET, N is usually a fixed constant, so that the sCRB turns into the familiar MSE per reconstruction datum. For sufficiently large coherent-state data N and densely sampled phase-space points, one can show that the MSE for UHOM goes as the average shot-noise limit ($\propto 1/\mathbb{E}[N]$), which again reminds us that the accuracy of $\widehat{\boldsymbol{q}}$ varies only with the *used* reconstruction data sample size, as always. It then follows that $\inf_{\widehat{\boldsymbol{q}}}\{\mathbb{E}[N(\widehat{\boldsymbol{q}}-\boldsymbol{q})^2]\}=\mathbb{E}[N]\inf_{\widehat{\boldsymbol{q}}}\{\mathbb{E}[(\widehat{\boldsymbol{q}}-\boldsymbol{q})^2]\}$.

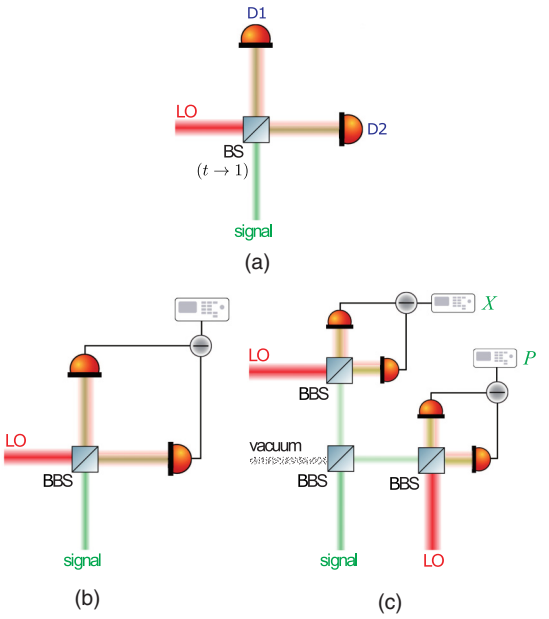

FIG. 1. Schema for the (a) UHOM, (b) BHOM, and (c) HET setups. The UHOM scheme consists only of one beam splitter (BS) that is almost perfectly transmissive (transmission amplitude $t\to 1$) and two photodetectors, D1 and D2, where only data corresponding to vacuum-state measurement with D1 are used to estimate the Husimi function, which is a significant experimental simplification compared to HET, which requires three balanced BSs (BBSs) and four photodetectors to randomly sample the Husimi function.

This means that while the comparisons of the sampling methods are made by scaling away the used reconstruction data, it should not matter whether this scaling is done for every experiment or with an overall average data cost for all the experiments. Any physically meaningful definition of the tomographic power should be invariant under such a technical variation [43].

III. MAIN RESULTS

Both the delocalized (HET) and the localized (UHOM) phase-space sampling methods share a common trait: their data $N=\sum_l n_l$ directly reconstruct the Husimi function $Q(\alpha)$: $n_l/\sum_l n_l\approx(\delta\alpha)Q(\alpha_l)/\pi$ at a sampled $\alpha=\alpha_l$ for some small prechosen area $(\delta\alpha)$ of the sampled discretized phase space. Therefore the Husimi representation of $\boldsymbol{q}$ in (1) invites an estimator of the form $\widehat{\boldsymbol{q}}=\sum_l n_l\,\boldsymbol{v}_{\rm P}(\alpha_l)/\sum_l n_l$. Furthermore, such a sample average estimator, for these HET and UHOM data, follows a multivariate Gaussian distribution in the limit of large N with the correct mean $\boldsymbol{q}$ and data covariance, so that $\widehat{\boldsymbol{q}}$ achieves the sCRB asymptotically. After a proper statistical analysis for $N\gg 1$ and a densely sampled α_ls, we have the intuitively simple expressions (see Appendixes A and B for the derivations and optimality arguments)

$$\mathrm{sCRB}_{\rm HET}=\int\frac{(d\alpha')}{\pi}Q(\alpha')[\boldsymbol{v}_{\rm P}(\alpha')-\boldsymbol{q}]^2,$$
$$\mathrm{sCRB}_{\rm UHOM}=\int\frac{(d\alpha')}{\pi}Q(\alpha')[1-Q(\alpha')][\boldsymbol{v}_{\rm P}(\alpha')-\boldsymbol{q}]^2. \quad (3)$$

By inspection, since $Q(\alpha)[1-Q(\alpha)] \leqslant Q(\alpha)$ for any ρ, we immediately find that $\mathrm{sCRB}_{\mathrm{UHOM}} < \mathrm{sCRB}_{\mathrm{HET}}$. This first general result has important physical implications. It shows that localized sampling always reduces the magnitude of the phase-space distribution via the binomial deformation $Q(\alpha) \to Q(\alpha)[1-Q(\alpha)]$. This leads to a smaller combined reconstruction variance per datum for any list of parameters $\boldsymbol{q}$ relative to HET. In practice, the tomographic advantages of localized binomial phase-space sampling are realized with only a replacement of the balanced BS with a highly transmissive BS, which is a minor adjustment of the BHOM setup in Fig. 1(b). For realistic photodetectors of efficiency $0 < \eta \leqslant 1$ and modeled with an average signal-uncorrelated dark-count rate c, using the definition $p_c(\alpha,\eta) = \langle {:}e^{-\eta(a^\dagger-\alpha)(a-\alpha)-c}{:}\rangle \leqslant 1$, where a is the usual photonic ladder operator, $:\cdot:$ denotes operator normal ordering, $p(\alpha,\eta) \equiv p_{c=0}(\alpha,\eta)$, and the sampled probabilities with HET are given by $\eta p(\alpha,\eta)$, while the binomial probability for no-click events at photodetector D1 in UHOM is $p_c(\alpha,\eta)$ [22]. These give the more realistic bounds

$$\begin{aligned}\mathrm{sCRB}'_{\mathrm{HET}} &= \eta \int \frac{(d\alpha')}{\pi}\, p(\alpha',\eta)[\boldsymbol{v}_{\mathrm{P}}(\alpha') - \boldsymbol{q}]^2,\\ \mathrm{sCRB}'_{\mathrm{UHOM}} &= \eta \int \frac{(d\alpha')}{\pi}\, p(\alpha',\eta)[1-p_c(\alpha',\eta)][\boldsymbol{v}_{\mathrm{P}}(\alpha') - \boldsymbol{q}]^2,\end{aligned} \tag{4}$$

which satisfy $\mathrm{sCRB}'_{\mathrm{UHOM}} < \mathrm{sCRB}'_{\mathrm{HET}}$. [See Appendix C for the arguments that lead to Eq. (4). Furthermore, the bounds should diverge as $\eta \to 0$, which means that one cannot swap this limit with the phase-space integration.] It is interesting to point out that owing to the renormalization of the measured sampling events, the additional dark-count imperfections do not arbitrarily degrade the performance of UHOM but, rather, limit it to that of HET. That is, $\mathrm{sCRB}'_{\mathrm{UHOM}} \to \mathrm{sCRB}'_{\mathrm{HET}}$ as $c \to \infty$. The reason behind this limit is the multiplicative dark-count contribution to the detection probabilities (here in the form of an exponential of c), which is a common feature of uncorrelated dark counts with signal detection events. Evidently, this limit is valid when $N_0 \gg c$.

For an arbitrary $\boldsymbol{V}$ that is a complicated function of X and P, the general recipe for $\widehat{\boldsymbol{q}}$ with BHOM data is to adopt the Wigner representation in (1) and estimate $W(\alpha)$ by an application of the inverse Radon transform (invR) to the BHOM probabilities. Upon denoting the invR kernel $\mathscr{R}^{-1}_{\alpha}(x_\vartheta,\vartheta) = \int dk|k| \exp[ik(x\cos\vartheta + p\sin\vartheta - x_\vartheta)]$ for a given LO phase ϑ and voltage x_ϑ, the corresponding estimator for the BHOM data is given by $\widehat{\boldsymbol{q}} = \sum_{l,j,k} \mathscr{R}^{-1}_{\alpha_l}(x_j,\vartheta_k) n_{jk}\, \boldsymbol{v}_{\mathrm{W}}(\alpha_l) / \sum_{l,j,k} \mathscr{R}^{-1}_{\alpha_l}(x_j,\vartheta_k) n_{jk}$, where $n_{jk}/\sum_j n_{jk}$ estimates the BHOM probability $dx\, p(x_j,\vartheta_k)$. The tomographic power of BHOM for this general recipe with invR (only one kind of estimator considered here) is measured by

$$\begin{aligned}\mathrm{sCRB}_{\mathrm{BHOM}} &= \int \frac{(d\alpha')}{\pi} \int \frac{(d\alpha'')}{\pi} w_{\alpha',\alpha''}\\ &\quad \times [\boldsymbol{v}_{\mathrm{W}}(\alpha') - \boldsymbol{q}]\cdot[\boldsymbol{v}_{\mathrm{W}}(\alpha'') - \boldsymbol{q}],\\ w_{\alpha',\alpha''} &= \int_{(\pi)} \frac{d\vartheta}{2\pi} \int dx'_\vartheta \int dx''_\vartheta\, \mathscr{R}^{-1}_{\alpha'}(x'_\vartheta,\vartheta)\, \mathscr{R}^{-1}_{\alpha}(x''_\vartheta,\vartheta)\\ &\quad \times [p(x'_\vartheta,\vartheta)\delta(x'_\vartheta - x''_\vartheta) - p(x'_\vartheta,\vartheta)p(x''_\vartheta,\vartheta)].\end{aligned} \tag{5}$$

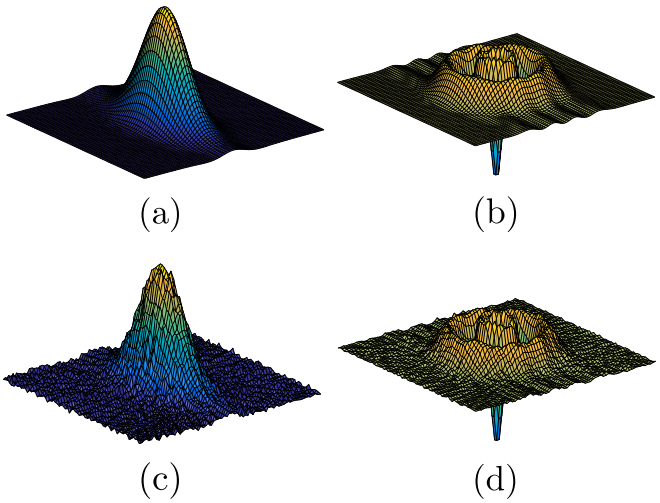

FIG. 2. Wigner functions of (a, c) a squeezed Gaussian state and (b, d) a Fock state of $n = 3$ reconstructed with a truncated invR for BHOM based on (a, b) perfect data and (c, d) noisy data. The wriggles of the reconstructed functions that come from truncations to a 50-dimensional Hilbert subspace, even for the case of perfect data, can lead to significant deviations from the true $\boldsymbol{q}$.

In practice, the estimation of the Wigner function $W(\alpha)$ is done in a truncated Hilbert space. As such, a direct application of the invR to the measured BHOM probabilities typically gives rise to $W(\alpha)$ with truncation phase-space wriggles that are otherwise absent in the infinite-dimensional limit. Together with the high sensitivity of invR to statistical fluctuations, $\mathrm{sCRB}_{\mathrm{BHOM}}$ is in general greater than either $\mathrm{sCRB}_{\mathrm{UHOM}}$ or $\mathrm{sCRB}_{\mathrm{HET}}$ (see Fig. 2). It is a separate matter with UHOM, where the data constitute the directly sampled Husimi function. As such, UHOM data are free of reconstruction artifacts and converge more quickly to the true Husimi function as N increases. Thus, for general parameters where $\boldsymbol{V}$ is a complicated function of X and P, UHOM is the best option. Although it is known that the maximum-likelihood method can reduce such reconstruction instabilities [44,45], analytical tomographic studies of such a nonlinear numerical method remain an open problem.

Certainly, a much more expedient and trusted way to estimate $\boldsymbol{q}$ (referred to as the BHOMOPT strategy) when $\boldsymbol{V}$ is a simple function of X and P is a direct and optimized data-processing strategy of the measured voltage values for every LO phase ϑ such that $\boldsymbol{q}$ can be efficiently reconstructed without having to go through any formal invR. For instance, in moment tomography [33,34,37], the entries of $\boldsymbol{q}$ are linearly related to the moments of the quadrature operator, $\langle X^m_\vartheta\rangle = \langle (X\cos\vartheta + P\sin\vartheta)^m\rangle$, sampled by BHOM. Therefore, $\mathrm{sCRB}_{\mathrm{BHOMOPT}}$ for any state using this improved reconstruction strategy can be obtained through the Fisher information on the homodyne parameter $\langle X^m_\vartheta\rangle$. The theory for this was developed in [34]. It shall be shown that, in practice, UHOM is tomographically more powerful than all other methods for moment tomography of interesting states, which forms the second main result.

If ideal photon-number-resolved detectors do exist, then one may certainly use all displaced-Fock-state data of UHOM

to reconstruct parameters. But it has to be done again with sophisticated nonlinear methods like maximum likelihood rather than simply first taking the data parity transform to obtain the Wigner function and then using this reconstructed to estimate observable parameters, the latter which shall introduce similarly large amplified errors as in the case of invR with BHOM data.

IV. MOMENT-TOMOGRAPHY ANALYSIS

We demonstrate the tomographic power of UHOM with moment tomography of orders $m = 1$ through $m = 4$. In particular, we study symmetrically ordered operator moments of X and P that appear naturally in high-order operator covariances. As examples, we consider two classes of quantum states. The first example is the class of (centralized) Gaussian states described by a covariance matrix of eigenvalues $\mu\lambda/2$ and $\mu/(2\lambda)$, where μ is related to the thermal mean photon number or temperature and λ describes the squeezing strength. For simplicity, we set $\mu = \lambda$, which approximately models strongly squeezed sources with accompanying excess noise associated with the antisqueezed quadrature due to realistic experimental imperfections (see Ref. [46]). The second example is the class of Fock states, which are arguably the most non-Glauber-Sudarshan-representable states. Even for these states, there is in general no known explicit expression for $\mathrm{sCRB}_{\mathrm{BHOM}}$ and numerical techniques are needed to calculate its values. See Appendix D for the list of expressions used in Figs. 3 and 4.

Figures 3 and 4 present the findings for these states. As intuitively expected, the more direct BHOMOPT reconstruction of the moments is always (exponentially) better than estimating the Wigner function with BHOM. Even then, this improved strategy still often underperforms in comparison to HET and UHOM. For the Gaussian states, when $m = 1$ or 3, marginalized sampling with BHOM and BHOMOPT gives the worst tomographic performance. Localized sampling with the UHOM strategy generates the most accurate estimators per reconstruction datum, and delocalized sampling with HET is second best. When $m = 2$ or 4, BHOMOPT beats HET, respectively, for $\mu \lesssim 1.262$ or $\mu \lesssim 1.017$, after which HET catches up in tomographic power, whereas UHOM ranks at the top in the respective range $\mu \gtrsim 1.04$ or $\mu \gtrsim 1.004$. Likewise for the Fock states, both HET and UHOM beat BHOM and BHOMOPT for all n values and $m = 1,3$. When $m = 2$ or 4, BHOMOPT initially outperforms HET for the vacuum state (and also the $n = 1$ state for $m = 2$) and subsequently becomes inferior to HET. UHOM, on the other hand, is superior to all methods in tomographic power for all $n > 0$.

That HET surpasses BHOMOPT in the $m = 1$ case for *any* state is a consequence of the Heisenberg-Robertson-Schrödinger uncertainty relation [34]. The limiting case where the two methods give identical sCRBs is when the state is of minimum uncertainty, yet UHOM is able to overcome this limit owing to the binomial variances. For a vacuum ($\mu = 1$ or $n = 0$), both UHOM and BHOMOPT are almost identical in power ($\mathrm{sCRB}_{\mathrm{UHOM}}/\mathrm{sCRB}_{\mathrm{BHOMOPT}} = 33/32 \approx 1.031$ and $9879/9856 \approx 1.002$ for $m = 2$ and 4) within experimental error margins. This justifies the use of UHOM essentially for all these states.

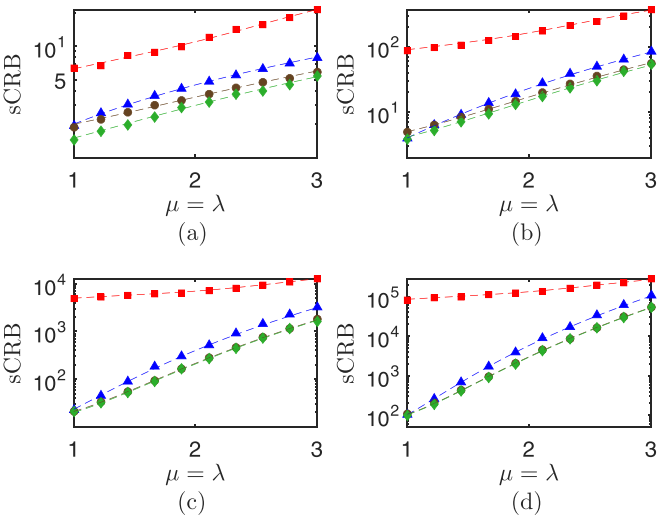

FIG. 3. Plots for the (a) first-, (b) second-, (c) third-, and (d) fourth-moment reconstructions of a Gaussian state of $1 \leqslant \mu = \lambda \leqslant 3$, in which the sCRB of BHOM (squares and curve), BHOMOPT (triangles and curve), HET (circles and curve), and UHOM (diamonds and curve) are illustrated. The instability and sensitivity of the invR with the BHOM marginalized sampling strategy are clear in the plots, which behavior also depends on the truncated Hilbert space. Evidently, UHOM exhibits a more superior tomographic power than HET, BHOM, and BHOMOPT. Dashed curves represent theory derived from (3) and (5), whereas symbols are computed with Monte Carlo simulated data of the CV experiments for a 50-dimensional Hilbert space. For the purpose of illustrating the results, we take $\eta = 1$ for simplicity.

V. CONCLUSIONS

We have first proven that, for every *used* reconstruction datum, localized phase-space sampling with unbalanced homodyning *always* beats delocalized phase-space sampling with

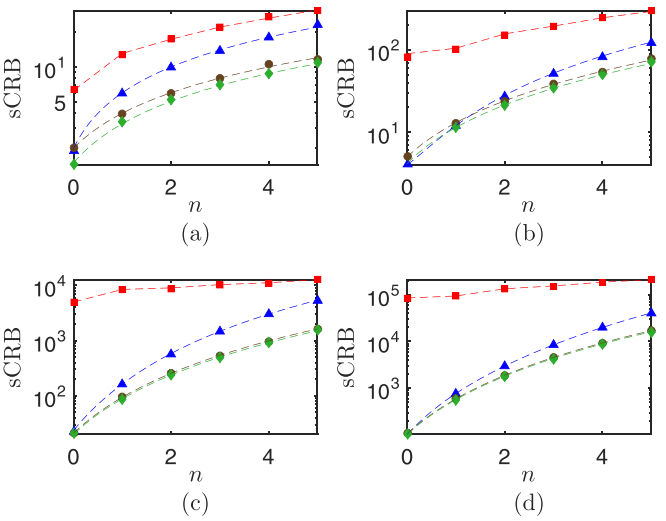

FIG. 4. Plots of sCRB for Fock states of $0 \leqslant n \leqslant 5$. All specifications follow those in Fig. 3. For each BHOM plot, the dashed curve joins the six theoretically calculated numerical values that match the squares.

heterodyning in tomographic power measured by the scaled Cramér-Rao for any quantum state and general multivariate observable-parameter tomography. The reason is the binomial nature of unbalanced homodyne data, which enhances the resolution of Husimi-function reconstruction with fewer experimental components. We have next demonstrated that for the Gaussian states and Fock states, localized sampling almost always beats marginalized sampling with balanced homodyning in moment tomography, except for the vacuum where both methods are practically equals. These findings shed light on the general performance of sampling methods in continuous-variable tomography.

ACKNOWLEDGMENTS

The author thanks D. Ahn, Z. Hradil, and J. Řeháček for illuminating discussions. This work was financially supported by the BK21 Plus Program (21A20131111123) funded by the Ministry of Education (MOE; Korea) and National Research Foundation of Korea (NRF), an NRF grant funded by the Korean government (MSIP; Grant No. 2010-0018295), the KIST Institutional Program (Project No. 2E26680-16-P025), and the Spanish MINECO (Grant No. FIS2015-67963-P).

APPENDIX A: DERIVATIONS OF EQS. (2) AND (4)

To arrive at the expression for $\mathrm{sCRB}_{\mathrm{HET}}$, we first note that since N is fixed for HET, it is sufficient to use the standard formula $\mathbb{E}[n_l n_{l'}] = N p_l \delta_{l,l'} + N(N-1) p_l p_{l'}$ for the binned multinomial HET data with $p_l \approx (d\alpha) Q(\alpha_l)/\pi$. For UHOM, we would need the averages

$$\mathbb{E}\left[\frac{n_l}{N}\right] = \frac{p_l}{\sum_l p_l} - \frac{\sigma_l^2}{\left(\sum_l p_l\right)^2} + \frac{p_l}{\left(\sum_l p_l\right)^3} \sum_{l'} \sigma_{l'}^2, \tag{A1}$$

$$\mathbb{E}\left[\frac{n_l n_{l'}}{N^2}\right] = \frac{\sigma_l^2 \delta_{l,l'} + p_l p_{l'}}{\left(\sum_l p_l\right)^2} - \frac{2\left(p_l \sigma_{l'}^2 + p_{l'} \sigma_l^2\right)}{\left(\sum_l p_l\right)^3} + \frac{3 p_l p_{l'}}{\left(\sum_l p_l\right)^4} \sum_{l''} \sigma_{l''}^2, \tag{A2}$$

where here p_l is instead equal to $Q(\alpha_l)$, $\sigma_l^2 = p_l(1-p_l)/N_0$, and N_0 is the total number of detection events for each α_l.

The averages of data ratios in Eqs. (A1) and (A2) can be straightforwardly derived by starting with this easy but crucial integral identity,

$$\frac{1}{A} = -i \int_0^\infty dt\, e^{itA - \epsilon t}\Big|_{\epsilon=0}, \tag{A3}$$

for any nonzero A. We can then rewrite the UHOM ratio averages as

$$\mathbb{E}\left[\frac{f_l}{\sum_l f_l}\right] = -\int_0^\infty dt \frac{\partial}{\partial \lambda_l} \mathbb{E}\left[e^{i \sum_l \lambda_l f_l}\right]\Big|_{\lambda_l = t},$$

$$\mathbb{E}\left[\frac{f_l f_{l'}}{\left(\sum_l f_l\right)^2}\right] = \int_0^\infty dt \int_0^\infty dt' \frac{\partial}{\partial \lambda_l} \frac{\partial}{\partial \lambda_{l'}} \mathbb{E}\left[e^{i \sum_l \lambda_l f_l}\right]\Big|_{\lambda_l = t + t'} \tag{A4}$$

after an equivalent renormalization $f_l = n_l/N_0$ for notational simplicity. The central object to be evaluated is thus the characteristic function $\mathbb{E}[e^{i \sum_l \lambda_l f_l}]$. As the data for distinct α_l are statistically independent, we may proceed with the decomposition

$$\mathbb{E}\left[e^{i \sum_l \lambda_l f_l}\right] = \prod_l \mathbb{E}[e^{i \lambda_l f_l}], \tag{A5}$$

where central limit theorem gives

$$\mathbb{E}[e^{i \lambda_l f_l}] = e^{-\frac{1}{2}\lambda_l^2 \sigma_l^2 + i \lambda_l p_l} \tag{A6}$$

for $N_0 \gg 1$, and the corresponding integrals

$$\mathbb{E}\left[\frac{f_l}{\sum_l f_l}\right] = -\int_0^\infty dt\, e^{-at^2 + ibt} \left(i p_l - t \sigma_l^2\right) \tag{A7}$$

and

$$\mathbb{E}\left[\frac{f_l f_{l'}}{\left(\sum_l f_l\right)^2}\right] = \int_0^\infty dt \int_0^\infty dt'\, e^{-a(t+t')^2 + ib(t+t')} \times [c_1 (t+t')^2 - i c_2 (t+t') - c_3], \tag{A8}$$

where the parameters are now $\sigma_l^2 = p_l(1-p_l)$, $a = \sum_l \sigma_l^2/2$, $b = \sum_l p_l$, $c_1 = \sigma_l^2 \sigma_{l'}^2$, $c_2 = p_l \sigma_{l'}^2 + p_{l'} \sigma_l^2$, and $c_3 = p_l p_{l'} + \delta_{l,l'} \sigma_l^2$. The answers to these integrals involve the imaginary error function $\mathrm{erfi}(b/2\sqrt{a})$, and in the limit of large sample size where $b \gg 2\sqrt{a}$, it turns out that the asymptotic expansion

$$\sqrt{\pi}\, e^{-\frac{b^2}{4a}} \mathrm{erfi}\left(\frac{b}{2\sqrt{a}}\right) \approx \frac{24 a^{5/2}}{b^5} + \frac{4 a^{3/2}}{b^3} + \frac{2\sqrt{a}}{b} \tag{A9}$$

gives Eqs. (A1) and (A2) for sufficiently dense sampling ($0 < b \gg 1$). The integral expressions for $\mathrm{sCRB}_{\mathrm{HET}}$ and $\mathrm{sCRB}_{\mathrm{UHOM}}$ are the acquired limits of such a dense sampling.

The important technical statement $\min_{\widehat{\boldsymbol{q}}}\{\mathbb{E}[N(\widehat{\boldsymbol{q}} - \boldsymbol{q})^2]\} = \mathbb{E}[N] \min_{\widehat{\boldsymbol{q}}}\{\mathbb{E}[(\widehat{\boldsymbol{q}} - \boldsymbol{q})^2]\}$ is then easily proven with the additional statistical identity

$$\mathbb{E}\left[\frac{n_l n_{l'}}{N}\right] = \frac{\sigma_l^2 \delta_{l,l'} + p_l p_{l'}}{\sum_l p_l} - \frac{p_l \sigma_{l'}^2 + p_{l'} \sigma_l^2}{\left(\sum_l p_l\right)^2} + \frac{p_l p_{l'}}{\left(\sum_l p_l\right)^3} \sum_{l''} \sigma_{l''}^2, \tag{A10}$$

which can also be derived with

$$\mathbb{E}\left[\frac{f_l f_{l'}}{\sum_l f_l}\right] = \int_0^\infty dt\, e^{-at^2 + ibt} [c_1 t^2 - i c_2 t - c_3] \tag{A11}$$

of the same parameters defined above after a similar calculation.

To get $\mathrm{sCRB}_{\mathrm{BHOM}}$, we need the data-ratio averages

$$\mathbb{E}\left[\frac{n_{jk}}{\mathscr{N}}\right] = \frac{p_{jk}}{b} + \frac{2 a p_{jk}}{b^3} - \frac{w_{jk}}{b^2}, \tag{A12}$$

$$\mathbb{E}\left[\frac{n_{jk} n_{j'k'}}{\mathscr{N}^2}\right] = \frac{p_{jk} p_{j'k'} + \delta_{j,j'} \Sigma_{jkk'}}{b^2} + \frac{6 a p_{jk} p_{j'k'}}{b^4} - \frac{2}{b^3}(p_{jk} w_{j'k'} + p_{j'k'} w_{jk}), \tag{A13}$$

which hold when BHOM sampling is sufficiently dense ($|b| \gg 1 \Rightarrow N \gg 1$), with $\mathscr{N} = \sum_l \sum_{j=1}^{n_\vartheta} \sum_{k=1}^{n_x} \mathscr{R}_{ljk}^{-1} n_{jk}$, $p_{jk} = dx_k\, p(x_k, \vartheta_j)$, $\widetilde{N} = \sum_{k=1}^{n_x} n_{jk}$, $\Sigma_{jkk'} = (p_{jk}\delta_{k,k'} - p_{jk} p_{jk'})/\widetilde{N}$, $w_{jk} = \sum_{k',l'} \mathscr{R}_{l'jk'}^{-1} \Sigma_{jkk'}$, $a = \sum_{j,k,l} \mathscr{R}_{ljk}^{-1} w_{jk}/(4 n_\vartheta)$, and $b = \sum_{j,k,l} \mathscr{R}_{ljk}^{-1} p_{jk}/(2 n_\vartheta)$. The averages in (A12) and (A13) can

be verified with (A3), which yields

$$\mathbb{E}\left[\frac{f_{jk}}{\sum_{l,j,k}\mathscr{R}^{-1}_{ljk}f_{jk}}\right] = -i\int_0^\infty dt\ \mathbb{E}\left[f_{jk}e^{it\sum_{l,j,k}\mathscr{R}^{-1}_{ljk}f_{jk}}\right] \tag{A14}$$

$$= -\int_0^\infty dt\,\frac{\partial}{\partial\lambda_{ljk}}\mathbb{E}\left[e^{i\sum_{l,j,k}\lambda_{ljk}f_{jk}}\right]\Big|_{\lambda_{ljk}=t\mathscr{R}^{-1}_{ljk}} \tag{A15}$$

and

$$\mathbb{E}\left[\frac{f_{jk}\,f_{j'k'}}{\left(\sum_{l,j,k}\mathscr{R}^{-1}_{ljk}f_{jk}\right)^2}\right] = -\int_0^\infty dt\int_0^\infty dt'\ \mathbb{E}\left[f_{jk}f_{j'k'}e^{i(t+t')\sum_{l,j,k}\mathscr{R}^{-1}_{ljk}f_{jk}}\right] = \int_0^\infty dt\int_0^\infty dt'\,\frac{\partial}{\partial\lambda_{ljk}}\frac{\partial}{\partial\lambda_{l'j'k'}} \times\ \mathbb{E}\left[e^{i\sum_{l,j,k}\lambda_{ljk}f_{jk}}\right]\Big|_{\lambda_{ljk}=(t+t')\mathscr{R}^{-1}_{ljk}} \tag{A16}$$

after a renormalization $f_{jk}=n_{jk}/\widetilde{N}$ with the constant $\widetilde{N}$.

We again realize that the data for distinct ϑ_j are statistically independent, which means that

$$\mathbb{E}\left[e^{i\sum_{l,j,k}\lambda_{ljk}f_{jk}}\right] = \prod_{j=1}^{n_\vartheta}\mathbb{E}\left[e^{i\sum_{l,k}\lambda_{ljk}f_{jk}}\right] \tag{A17}$$

decomposes into the independent characteristic functions. Because the binned data $\{n_{jk}\}_k$ for every j follows a multinomial distribution defined by the BHOM quantum probabilities $\sum_k p_{jk}=1$, in the limit of large $\widetilde{N}$, the column $\boldsymbol{f}_j=(f_{jk})$ follows a Gaussian distribution of mean $\boldsymbol{p}_j$ and covariance matrix $[\mathrm{diag}(\boldsymbol{p}_j)-\boldsymbol{p}_j\boldsymbol{p}_j]/\widetilde{N}$, so that

$$\mathbb{E}\left[e^{i\sum_{l,k}\lambda_{ljk}f_{jk}}\right] = e^{-\frac{1}{2}\sum_{l,l',k,k'}\lambda_{ljk}\lambda_{l'jk'}\Sigma_{jkk'}+i\sum_{l,k}\lambda_{ljk}p_{jk}} \tag{A18}$$

according to the central limit theorem. After the differentiations, we have

$$\mathbb{E}\left[\frac{f_{jk}}{\sum_{l,j,k}\mathscr{R}^{-1}_{ljk}f_{jk}}\right] = -\int_0^\infty dt\,e^{-at^2+ibt}\,(ip_{jk}-tw_{jk}) \tag{A19}$$

and

$$\mathbb{E}\left[\frac{f_{jk}\,f_{j'k'}}{\left(\sum_{l,j,k}\mathscr{R}^{-1}_{ljk}f_{jk}\right)^2}\right] = \int_0^\infty dt\int_0^\infty dt'\,e^{-a(t+t')^2+ib(t+t')} \times\ [c_1(t+t')^2-ic_2(t+t')-c_3], \tag{A20}$$

where $c_1=w_{jk}w_{j'k'}$, $c_2=p_{jk}w_{j'k'}+p_{j'k'}w_{jk}$, and $c_3=p_{jk}p_{j'k'}+\delta_{j,j'}\Sigma_{jkk'}$. From the asymptotic formula in (A9) that holds for $N\gg 1$, we arrive at the results in Eqs. (A12) and (A12) up to $O(1/N)$ as long as phase-space sampling is sufficiently dense or $|b|\gg 1$.

APPENDIX B: ASYMPTOTIC INDEPENDENCE OF UHOM RANDOM VARIABLES

Let $z_l\equiv n_l/N$. Then for any two UHOM random variables z_l and $z_{l'}$, the one-dimensional version of Kac's theorem [47] states that if we can show that the two-dimensional characteristic function

$$\mathbb{E}[\exp(i(k_lz_l+k_{l'}z_{l'}))] = \mathbb{E}[\exp(ik_lz_l)]\,\mathbb{E}[\exp(ik_{l'}z_{l'})] \tag{B1}$$

satisfies this decomposition rule for all real k_l and $k_{l'}$, then z_l and $z_{l'}$ are statistically independent, and vice versa. This is equivalent to showing that $\mathbb{E}[z_l^m z_{l'}^{m'}]=\mathbb{E}[z_l^m]\mathbb{E}[z_{l'}^{m'}]$ for any $l,l'\neq l$, m, and m'.

For sufficiently large N_0, the first-order Taylor expansion in n_l about N_0p_l well approximates

$$\frac{1}{\left(\sum_l n_l\right)^{m+m'}} \approx \frac{(m+m'+1)N_0\sum_l p_l-(m+m')\sum_l n_l}{\left(N_0\sum_l p_l\right)^{m+m'+1}}. \tag{B2}$$

Then by recalling the simple statistical fact that the n_l's of distinct l are of course independent binomial random variables,

$$\mathbb{E}\left[z_l^m z_{l'}^{m'}\right] \approx \frac{m+m'+1}{\left(N_0\sum_l p_l\right)^{m+m'}}\mathbb{E}\left[n_l^m\right]\mathbb{E}\left[n_{l'}^{m'}\right] - \frac{m+m'}{\left(N_0\sum_l p_l\right)^{m+m'+1}}\mathbb{E}\left[\sum_{l''}n_{l''}n_l^m n_{l'}^{m'}\right], \tag{B3}$$

where

$$\mathbb{E}\left[\sum_{l''}n_{l''}n_l^m n_{l'}^{m'}\right] = N_0\sum_{l''\neq l\&l'}p_{l''}\mathbb{E}\left[n_l^m\right]\mathbb{E}\left[n_{l'}^{m'}\right] + \mathbb{E}\left[n_l^{m+1}\right]\mathbb{E}\left[n_{l'}^{m'}\right]+\mathbb{E}\left[n_l^m\right]\mathbb{E}\left[n_{l'}^{m'+1}\right]. \tag{B4}$$

Since from Appendix A, we know that n_l/N_0 is a Gaussian random variable of mean $\mu_l=p_l$ and variance $\sigma_l^2=p_l(1-p_l)/N_0$ for $N_0\gg 1$, the mth moment

$$\mathbb{E}\left[n_l^m\right] = \left(N_0\frac{\sigma_l}{\sqrt{2}\,i}\right)^m \mathrm{H}_m\left(i\,\frac{\mu_l}{\sqrt{2}\sigma_l}\right) \tag{B5}$$

is a simple function of the mth-degree Hermite polynomial $\mathrm{H}_m(\cdot)$. Using the simple relation $\mathrm{H}_{m+1}(y)=2y\,\mathrm{H}_m(y)-2m\,\mathrm{H}_{m-1}(y)$, which permits changes in the polynomial degree, we obtain the useful identity

$$\mathbb{E}\left[n_l^{m+1}\right] = \mu_lN_0\mathbb{E}\left[n_l^m\right]+(m+1)(N_0\sigma_l)^2\mathbb{E}\left[n_l^{m-1}\right], \tag{B6}$$

which can now be applied to Eq. (B5) to get

$$\mathbb{E}\left[\sum_{l''}n_{l''}n_l^m n_{l'}^{m'}\right] = \mathbb{E}\left[\sum_{l''}n_{l''}\right]\mathbb{E}\left[n_l^m\right]\mathbb{E}\left[n_{l'}^{m'}\right] + (m+1)(N_0\sigma_l)^2\mathbb{E}\left[n_l^{m-1}\right]\mathbb{E}\left[n_{l'}^{m'}\right] + (m'+1)(N_0\sigma_l)^2\mathbb{E}\left[n_l^m\right]\mathbb{E}\left[n_{l'}^{m'-1}\right]. \tag{B7}$$

For sufficiently dense sampling the sum $\sum_l n_l$ should also be independent of n_l since the sum is contributed by very many terms that are all distinct and therefore independent of

n_l. Using the asymptotic relation $\mathrm{H}_m(y) \approx (2y)^m$ for $y \gg 1$, we find that

$$\mathbb{E}\big[z_l^m z_{l'}^{m'}\big] \approx \mathbb{E}\left[\frac{1}{\big(\sum_l n_l\big)^{m+m'}}\right]\mathbb{E}\big[n_l^m\big]\mathbb{E}\big[n_{l'}^{m'}\big] - \frac{(m+m')p_l^m p_{l'}^{m'}}{\mathbb{E}[N]\big(\sum_l p_l\big)^{m+m'}} f_{m,m'}(p_l,p_{l'}), \tag{B8}$$

where $f_{m,m'}(x,y) = (m+1)(1-x) + (m'+1)(1-y)$. The next order in the asymptotic expansion of $\mathrm{H}_m(y)$ gives a smaller correction to $\mathbb{E}[z_l^m z_{l'}^{m'}]$.

We can repeat the exercise and obtain the asymptotic formulas

$$\mathbb{E}\left[\frac{n_{l'}^{m'}}{\big(\sum_l n_l\big)^m}\right] \approx \mathbb{E}\left[\frac{1}{\big(\sum_l n_l\big)^m}\right]\mathbb{E}\big[n_{l'}^{m'}\big] - \frac{m(m'+1)(1-p_{l'})}{\mathbb{E}[N]}\frac{(N_0 p_{l'})^{m'}}{\big(N_0\sum_l p_l\big)^m} \tag{B9}$$

and

$$\mathbb{E}\left[\frac{1}{\big(\sum_l n_l\big)^{m+m'}}\right] \approx \mathbb{E}\left[\frac{1}{\big(\sum_l n_l\big)^m}\right]\mathbb{E}\left[\frac{1}{\big(\sum_l n_l\big)^{m'}}\right] + \frac{2mm'}{(\mathbb{E}[N])^{m+m'+2}}\sum_l p_l(1-p_l), \tag{B10}$$

the latter is obtained from the second-order Taylor expansion of $1/(\sum_l n_l)^{m+m'}$ in n_l about $N_0 p_l$,

$$\mathbb{E}\left[\frac{1}{\big(\sum_l n_l\big)^{m+m'}}\right] \approx \frac{1}{(\mathbb{E}[N])^{m+m'}} + (N_0\sigma_l)^2\frac{(m+m')(m+m'+1)}{(\mathbb{E}[N])^{m+m'+2}}, \tag{B11}$$

in which the first-order term vanishes since $\mathbb{E}[n_l] = N_0 p_l$. These relations inform us that all statistical biases are asymptotic in nature. Combining all elements and keeping terms up to first order in $1/\mathbb{E}[N]$ gives

$$\mathbb{E}\big[z_l^m z_{l'}^{m'}\big] \approx \mathbb{E}\big[z_l^m\big]\mathbb{E}\big[z_{l'}^{m'}\big] + O\left(\frac{1}{\mathbb{E}[N]\big(\sum_l p_l\big)^{m+m'}}\right). \tag{B12}$$

Finally, invoking Kac's theorem confirms asymptotic independence between z_l and $z_{l'}$ and, thereafter, for the whole set $\{z_l\}$ of these UHOM random variables.

APPENDIX C: REALISTIC DETECTIONS

It is a simple matter to show that the first main result remains unchanged for realistic detections. Suppose that all photodetectors now have the efficiency $0 \leqslant \eta \leqslant 1$ and an average dark-count rate c, so that we may model the realistic photon-number operator as $\eta\, a^\dagger a + c$ in the absence of signal-correlated dark counts due to afterpulsing. For this model, HET experiences no average dark-count effects due to photocurrent subtraction. Then standard characteristic-function treatment (see, for instance, [48]) allows us to find that the more realistic measured outcomes for HET are, instead of the usual coherent states $|\alpha\rangle\langle\alpha^*|$, given by the full-rank statistical mixtures

$$\frac{\eta}{1-\eta}\int\frac{(d\alpha')}{\pi}|\alpha'\rangle e^{-\frac{\eta}{1-\eta}|\alpha-\alpha'|^2}\langle\alpha'^*| = \eta{:}e^{-\eta(a^\dagger-\alpha^*)(a-\alpha)}{:}. \tag{C1}$$

Alternatively, Born's rule dictates that the realistic HET setup is equivalently the perfect HET setup with quantum state ρ transformed to ρ' by a corresponding Gaussian twirling operation. Then the expression $\mathrm{sCRB}'_{\mathrm{HET}}$ in (3) can be obtained by the simple replacement $\rho \to \rho'$.

For UHOM, the results in [22] show that the binomial probability for "no-click" detections is transformed to $p_c(\alpha,\eta) = \langle{:}e^{-\eta(a^\dagger-\alpha^*)(a-\alpha)-c}{:}\rangle$. The prefactor e^{-c} is a special case of the more general consideration of nonafterpulsing dark counts. Furthermore, in going from the discretized sum to the continuous integral limit, we note that $\sum_l p'_l = \sum_l p(\alpha_l,\eta) \to \pi\, e^{-c}/[(d\alpha)\eta]$, which contributes the multiplicative factor η in the expression for $\mathrm{sCRB}'_{\mathrm{UHOM}}$.

APPENDIX D: MOMENT TOMOGRAPHY

It is easily verified that for the mth operator moment ($m \geqslant l$), which is Weyl ordered in the position X and momentum P, its corresponding Wigner function is given by $x^l p^{m-l}$ in terms of the phase-space variables x and p. There is then a simple one-to-one relation between $\boldsymbol{v}_{\mathrm{P}}(\alpha)$ and $\boldsymbol{v}_{\mathrm{W}}(\alpha)$ as a consequence of the Gauss transform. These are given by

$$\boldsymbol{v}_{\mathrm{W}}(\alpha) \widehat{=} \begin{pmatrix} x \\ p \end{pmatrix} \leftrightarrow \boldsymbol{v}_{\mathrm{P}}(\alpha) \widehat{=} \begin{pmatrix} x \\ p \end{pmatrix},$$

$$\boldsymbol{v}_{\mathrm{W}}(\alpha) \widehat{=} \begin{pmatrix} x^2 \\ xp \\ p^2 \end{pmatrix} \leftrightarrow \boldsymbol{v}_{\mathrm{P}}(\alpha) \widehat{=} \begin{pmatrix} x^2 - \frac{1}{2} \\ xp \\ p^2 - \frac{1}{2} \end{pmatrix},$$

$$\boldsymbol{v}_{\mathrm{W}}(\alpha) \widehat{=} \begin{pmatrix} x^3 \\ x^2 p \\ xp^2 p^3 \end{pmatrix} \leftrightarrow \boldsymbol{v}_{\mathrm{P}}(\alpha) \widehat{=} \begin{pmatrix} x^3 - \frac{3}{2}x \\ x^2 p - \frac{1}{2}p \\ xp^2 - \frac{1}{2}x \\ p^3 - \frac{3}{2}p \end{pmatrix},$$

$$\boldsymbol{v}_{\mathrm{W}}(\alpha) \widehat{=} \begin{pmatrix} x^4 \\ x^3 p \\ x^2 p^2 \\ xp^3 \\ p^4 \end{pmatrix} \leftrightarrow \boldsymbol{v}_{\mathrm{P}}(\alpha) \widehat{=} \begin{pmatrix} x^4 - 3x^2 + \frac{3}{4} \\ x^3 p - \frac{3}{2}xp \\ x^2 p^2 - \frac{1}{2}x^2 - \frac{1}{2}p^2 + \frac{1}{4} \\ xp^3 - \frac{3}{2}xp \\ p^4 - 3p^2 + \frac{3}{4} \end{pmatrix}. \tag{D1}$$

Then the evaluation of $\mathrm{sCRB}_{\mathrm{BHOMOPT}}$, $\mathrm{sCRB}_{\mathrm{HET}}$, and $\mathrm{sCRB}_{\mathrm{UHOM}}$ amounts to the evaluation of all integrals involving $\boldsymbol{v}_{\mathrm{P}}(\alpha)$ and $\boldsymbol{v}_{\mathrm{W}}(\alpha)$ using the identities in (D1).

For $\mathrm{sCRB}_{\mathrm{HET}}$ and $\mathrm{sCRB}_{\mathrm{UHOM}}$, this can be easily accomplished with the help of characteristic functions $\chi_1 = \overline{e^{g^*\alpha + g\alpha^*}}$ [$g = (u+iv)/\sqrt{2}$] and $\chi_2 = \overline{\overline{e^{g^*\alpha + g\alpha^*}}}$, where the single and double overlines, respectively, denote the phase-

space integrals with respect to $Q(\alpha)$ and (unnormalized) $Q(\alpha)[1-Q(\alpha)]$. Then

$$\overline{x^k p^l} = \left(\frac{\partial}{\partial u}\right)^k \left(\frac{\partial}{\partial v}\right)^l \chi_1\Big|_{u,v=0},$$
$$\overline{\overline{x^k p^l}} = \left(\frac{\partial}{\partial u}\right)^k \left(\frac{\partial}{\partial v}\right)^l \chi_2\Big|_{u,v=0} \tag{D2}$$

supply the required quantities.

The centralized Gaussian states of the Husimi-function covariance matrix $\boldsymbol{G}_{\rm HET}$ have the characteristic functions

$$\chi_1 = \exp\left(\frac{\det\{\boldsymbol{G}_{\rm HET}\}}{2}\boldsymbol{g}^\dagger \boldsymbol{M}\,\boldsymbol{g}\right),$$
$$\chi_2 = \frac{1}{2\sqrt{\det\{\boldsymbol{G}_{\rm HET}\}}}\exp\left(\frac{\det\{\boldsymbol{G}_{\rm HET}\}}{4}\boldsymbol{g}^\dagger \boldsymbol{M}\,\boldsymbol{g}\right), \tag{D3}$$

where $\boldsymbol{g} \widehat{=} (-g \;\; g^*)^{\rm T}$, $\boldsymbol{M} = \boldsymbol{H}^\dagger \boldsymbol{G}_{\rm HET}^{-1}\boldsymbol{H}$, and $\boldsymbol{H} \widehat{=} \frac{1}{\sqrt{2}}\left(\begin{smallmatrix} 1 & 1 \\ -i & i \end{smallmatrix}\right)$. Those of the Fock states read

$$\chi_1 = e^{|g|^2}\,{\rm L}_n(-|g|^2),$$
$$\chi_2 = \frac{1}{2^{2n+1}}\binom{2n}{n} e^{\frac{|g|^2}{2}}\,{\rm L}_{2n}\left(-\frac{|g|^2}{2}\right). \tag{D4}$$

For the setting $\mu = \lambda$, the sCRB expressions are cataloged as follows:

$$\begin{aligned}
{\rm sCRB}_{1,\rm HET} &= \frac{1}{2}(3+\mu^2),\\
{\rm sCRB}_{1,\rm UHOM} &= {\rm sCRB}_{1,\rm HET} - \frac{3+\mu^2}{4\sqrt{2+2\mu^2}},\\
{\rm sCRB}_{2,\rm HET} &= \frac{1}{2}(6+3\mu^2+\mu^4),\\
{\rm sCRB}_{2,\rm UHOM} &= {\rm sCRB}_{2,\rm HET} - \frac{17+8\mu^2+3\mu^4}{16\sqrt{2+2\mu^2}},\\
{\rm sCRB}_{3,\rm HET} &= \frac{1}{8}\left(85+35\mu^2+33\mu^4+15\mu^6\right),\\
{\rm sCRB}_{3,\rm UHOM} &= {\rm sCRB}_{3,\rm HET} - \frac{77+21\mu^2+15\mu^2+15\mu^4}{64\sqrt{2+2\mu^2}},\\
{\rm sCRB}_{4,\rm HET} &= \frac{1}{8}(396+117\mu^2+148\mu^4+135\mu^6+48\mu^8),\\
{\rm sCRB}_{4,\rm UHOM} &= {\rm sCRB}_{4,\rm HET}\\
&\quad - \frac{735+142\mu^2+40\mu^4+234\mu^6+177\mu^8}{256\sqrt{2+2\mu^2}}.
\end{aligned} \tag{D5}$$

The corresponding expressions for the Fock states are given by

$$\begin{aligned}
{\rm sCRB}_{1,\rm HET} &= 2(n+1),\\
{\rm sCRB}_{1,\rm UHOM} &= {\rm sCRB}_{1,\rm HET} - \frac{\Gamma\left(n+\frac{3}{2}\right)}{\sqrt{\pi}\,\Gamma(n+1)},\\
{\rm sCRB}_{2,\rm HET} &= \frac{1}{2}(n+1)(3n+10),\\
{\rm sCRB}_{2,\rm UHOM} &= {\rm sCRB}_{2,\rm HET} - \binom{2n}{n}\frac{(n+1)(6n+7)}{2^{2n+3}},\\
{\rm sCRB}_{3,\rm HET} &= (n+1)\left(6n^2+20n+21\right),\\
{\rm sCRB}_{3,\rm UHOM} &= {\rm sCRB}_{3,\rm HET} - \frac{(6n^2+5n+4)\,\Gamma\left(n+\frac{3}{2}\right)}{2\sqrt{\pi}\,\Gamma(n+1)},\\
{\rm sCRB}_{4,\rm HET} &= \frac{1}{8}(n+1)(45n^3+437n^2+1040n+844),\\
{\rm sCRB}_{4,\rm UHOM} &= {\rm sCRB}_{4,\rm HET} - (n+1)\\
&\quad \times \frac{(180n^3+544n^2+521n+166)\,\Gamma\left(n+\frac{1}{2}\right)}{64\sqrt{\pi}\,\Gamma(n+1)}.
\end{aligned} \tag{D6}$$

The ${\rm sCRB}_{\rm BHOMOPT}$ expressions for the improved strategy of HOM can be found in an analogous way by looking at the operator moments and calculating the Fisher information matrix [34]. Further analysis shall be reported elsewhere but for now, we simply supply all the final analytical results that are obtainable from the theory. These are

$$\begin{aligned}
{\rm sCRB}_{1,\rm BHOMOPT} &= \tfrac{1}{2}(1+\mu)^2,\\
{\rm sCRB}_{2,\rm BHOMOPT} &= \tfrac{1}{4}(2+5\mu+2\mu^2+5\mu^3+2\mu^4),\\
{\rm sCRB}_{3,\rm BHOMOPT} &= \tfrac{5}{24}(9+30\mu+9\mu^2+16\mu^3+9\mu^4\\
&\quad +30\mu^5+9\mu^6),\\
{\rm sCRB}_{4,\rm BHOMOPT} &= 6+\tfrac{1}{6}\mu(\mu^2+1)\\
&\quad \times (153+36\mu-88\mu^2+153\mu^4+36\mu^5)
\end{aligned} \tag{D7}$$

for the Gaussian states and

$$\begin{aligned}
{\rm sCRB}_{1,\rm BHOMOPT} &= 2(2n+1),\\
{\rm sCRB}_{2,\rm BHOMOPT} &= 4(n^2+n+1),\\
{\rm sCRB}_{3,\rm BHOMOPT} &= \tfrac{14}{9}(20n^3+30n^2+40n+15),\\
{\rm sCRB}_{4,\rm BHOMOPT} &= \tfrac{77}{36}(17n^4+34n^3+139n^2+122n+48)
\end{aligned} \tag{D8}$$

for the Fock states.

[1] S. L. Braunstein and P. van Loock, Quantum information with continuous variables, Rev. Mod. Phys. **77**, 513 (2005).

[2] A. Ferraro, S. Olivares, and M. G. A. Paris, *Gaussian States in Continuous Variable Quantum Information* (Bibliopolis, Napoli, 2005).

[3] N. Cerf, G. Leuchs, and E. S. Polzik, eds., *Quantum Information with Continuous Variables of Atoms and Light* (Imperial College Press, London, 2007).

[4] U. L. Andersen, G. Leuchs, and C. Silberhorn, Continuous-variable quantum information processing, Laser Photon. Rev. **4**, 337 (2010).

[5] G. Adesso, S. Ragy, and A. R. Lee, Continuous variable quantum information: Gaussian states and beyond, Open Syst. Info. Dyn. **21**, 1440001 (2014).

[6] B. Coutinho dos Santos, K. Dechoum, and A. Z. Khoury, Continuous-Variable Hyperentanglement in a Parametric

Oscillator with Orbital Angular Momentum, Phys. Rev. Lett. **103**, 230503 (2009).
[7] K. Liu, J. Guo, C. Cai, S. Guo, and J. Gao, Experimental Generation of Continuous-Variable Hyperentanglement in an Optical Parametric Oscillator, Phys. Rev. Lett. **113**, 170501 (2014).
[8] H. P. Yuen and V. W. S. Chan, Noise in homodyne and heterodyne detection, Opt. Lett. **8**, 177 (1983).
[9] G. L. Abbas, V. W. S. Chan, and T. K. Yee, Local-oscillator excess-noise suppression for homodyne and heterodyne detection, Opt. Lett. **8**, 419 (1983).
[10] B. L. Schumaker, Noise in homodyne detection, Opt. Lett. **9**, 189 (1984).
[11] K. Vogel and H. Risken, Determination of quasiprobability distributions in terms of probability distributions for the rotated quadrature phase, Phys. Rev. A **40**, 2847 (1989).
[12] K. Banaszek and K. Wódkiewicz, Operational theory of homodyne detection, Phys. Rev. A **55**, 3117 (1997).
[13] E. Arthurs and J. L. Kelly, On the simultaneous measurement of a pair of conjugate observables, Bell Syst. Tech. J. **44**, 725 (1965).
[14] H. P. Yuen, Generalized quantum measurements and approximate simultaneous measurements of noncommuting observables, Phys. Lett. A **91**, 101 (1982).
[15] E. Arthurs and M. S. Goodman, Quantum Correlations: A Generalized Heisenberg Uncertainty Relation, Phys. Rev. Lett. **60**, 2447 (1988).
[16] H. Martens and W. M. de Muynck, The inaccuracy principle, Found. Phys. **20**, 357 (1990).
[17] H. Martens and W. M. de Muynck, Towards a new uncertainty principle: Quantum measurement noise, Phys. Lett. A **157**, 441 (1991).
[18] S. Stenholm, Simultaneous measurement of conjugate variables, Ann. Phys. **218**, 233 (1992).
[19] M. G. Raymer, Uncertainty principle for joint measurement of noncommuting variables, Am. J. Phys. **62**, 986 (1994).
[20] A. Trifonov, G. Björk, and J. Söderholm, Simultaneous Minimum-Uncertainty Measurement of Discrete-Valued Complementary Observables, Phys. Rev. Lett. **86**, 4423 (2001).
[21] R. F. Werner, The uncertainty relation for joint measurement of position and momentum, Quantum Info. Comput. **4**, 546 (2004).
[22] S. Wallentowitz and W. Vogel, Unbalanced homodyning for quantum state measurements, Phys. Rev. A **53**, 4528 (1996).
[23] K. Banaszek and K. Wódkiewicz, Direct Probing of Quantum Phase Space by Photon Counting, Phys. Rev. Lett. **76**, 4344 (1996).
[24] T. Opatrný and D.-G. Welsch, Density-matrix reconstruction by unbalanced homodyning, Phys. Rev. A **55**, 1462 (1997).
[25] T. Opatrný, D.-G. Welsch, S. Wallentowitz, and W. Vogel, Quantum state reconstruction by multichannel unbalanced homodyning, J. Mod. Opt. **44**, 2405 (1997).
[26] S. Wallentowitz, B. Seifert, and S. Godoy, Local sampling of the quantum phase-space distribution of a continuous-wave optical beam, New J. Phys. **14**, 105019 (2012).
[27] B. Kühn and W. Vogel, Unbalanced Homodyne Correlation Measurements, Phys. Rev. Lett. **116**, 163603 (2016).
[28] M. G. A. Paris, Displacement operator by beam splitter, Phys. Lett. A **217**, 78 (1996).
[29] T. Kiesel, Statistical analysis of sampling methods in quantum tomography, Phys. Rev. A **85**, 052114 (2012).
[30] J. Řeháček, Y. S. Teo, and Z. Hradil, Determining which quantum measurement performs better for state estimation, Phys. Rev. A **92**, 012108 (2015).
[31] D. Koutný, Y. S. Teo, Z. Hradil, and J. Řeháček, Fast universal performance certification of measurement schemes for quantum tomography, Phys. Rev. A **94**, 022113 (2016).
[32] J. Řeháček, Y. S. Teo, Z. Hradil, and S. Wallentowitz, Surmounting intrinsic quantum-measurement uncertainties in Gaussian-state tomography with quadrature squeezing, Sci. Rep. **5**, 12289 (2015).
[33] C. R. Müller, C. Peuntinger, T. Dirmeier, I. Khan, U. Vogl, Ch. Marquardt, G. Leuchs, L. L. Sánchez-Soto, Y. S. Teo, Z. Hradil, and J. Řeháček, Evading Vacuum Noise: Wigner Projections or Husimi Samples? Phys. Rev. Lett. **117**, 070801 (2016).
[34] Y. S. Teo, C. R. Müller, H. Jeong, Z. Hradil, J. Řeháček, and L. L. Sánchez-Soto, Superiority of heterodyning over homodyning: An assessment with quadrature moments, Phys. Rev. A **95**, 042322 (2017).
[35] S. Lorenz, N. Korolkova, and G. Leuchs, Continuous variable quantum key distribution using polarization encoding and post selection, Appl. Phys. B **79**, 273 (2004).
[36] A. M. Lance, T. Symul, V. Sharma, C. Weedbrook, T. C. Ralph, and P. K. Lam, No-Switching Quantum Key Distribution Using Broadband Modulated Coherent Light, Phys. Rev. Lett. **95**, 180503 (2005).
[37] J. Řeháček, S. Olivares, D. Mogilevtsev, Z. Hradil, M. G. A. Paris, S. Fornaro, V. D'Auria, A. Porzio, and S. Solimeno, Effective method to estimate multidimensional Gaussian states, Phys. Rev. A **79**, 032111 (2009).
[38] V. Scarani, H. Bechmann-Pasquinucci, N. J. Cerf, M. Dušek, N. Lütkenhaus, and M. Peev, The security of practical quantum key distribution, Rev. Mod. Phys. **81**, 1301 (2009).
[39] C. Weedbrook, S. Pirandola, R. García-Patrón, N. J. Cerf, T. C. Ralph, J. H. Shapiro, and S. Lloyd, Gaussian quantum information, Rev. Mod. Phys. **84**, 621 (2012).
[40] B.-G. Englert, *Lectures on Quantum Mechanics: Vol. 2. Simple Systems* (World Scientific, Singapore, 2006).
[41] K. E. Cahill and R. J. Glauber, Density operators and quasiprobability distributions, Phys. Rev. **177**, 1882 (1969).
[42] Without loss of generality, we only consider Hermitian $\boldsymbol{V}$s since any arbitrary complex observable $C = A + iB$ can be written as a linear combination of two Hermitian observables, $A = (C + C^\dagger)/2$ and $B = (C - C^\dagger)/(2i)$, so that reconstructing the single observable $\langle V\rangle = \langle C\rangle$ is equivalent to reconstructing the column $\langle \boldsymbol{V}\rangle = (\langle A\rangle\ \langle B\rangle)^{\mathrm{T}}$.
[43] The total input resources for UHOM include the unused data. Discussing input resources generally leads to equipment types and their error-convoluting effects with photon sources, which are beyond the scope of this article. For instance, BS stabilization in HET plays a major role in affecting the difficulty of copy generation relative to UHOM. As such, we focus on reconstruction statistics that involve only the *used data copies in all schemes* for fair and well-defined comparisons.
[44] K. Banaszek, Maximum-likelihood algorithm for quantum tomography, Acta Phys. Slov. **49**, 633 (1999).
[45] K. Banaszek, Quantum homodyne tomography with a priori constraints, Phys. Rev. A **59**, 4797 (1999).

[46] C. R. Müller, B. Stoklasa, C. Peuntinger, C. Gabriel, J. Řeháček, Z. Hradil, A. B. Klimov, G. Leuchs, Ch. Marquardt, and L. L. Sánchez-Soto, Quantum polarization tomography of bright squeezed light, New J. Phys. **14**, 085002 (2012).

[47] D. Applebaum, B. V. R. Bhat, J. Kustermans, and J. M. Lindsay, in *Quantum Independent Increment Processes I: From Classical Probability to Quantum Stochastic Calculus*. *Lecture Notes in Mathematics*, edited by M. Schuermann and U. Franz (Springer-Verlag, Berlin, 2005).

[48] Y. Lai and H. A. Haus, Characteristic functions and quantum measurements of optical observables, Quantum Opt. **1**, 99 (1989).